Sox9 Is Required for Nail-Bed Differentiation and Digit-Tip Regeneration

Miguel Lao[1], Alicia Hurtado[1,2], Alejandro Chacón de Castro[1], Miguel Burgos[1], Rafael Jiménez[1,3] and Francisco J. Barrionuevo[1,3]

The nail organ is a specialized appendage in which several ectodermal tissues coordinately function to sustain nail growth, a process that is coupled to digit regeneration. In this study, we show that the transcription factor *Sox9* is expressed in several cell populations in the mouse digit tip. We found a SOX9^{+} cell population in the nail bed, and genetic lineage tracing showed that this is a transient cell population differentiated from matrix nail stem cells. In the absence of *Sox9*, nail matrix stem cells fail to differentiate into epithelial nail-bed cells and proliferate, thus expanding distally and following the corneocyte fate, which results in outlandishly large fingernails. In addition, the tip of the underlying terminal phalanx undergoes bone regression. *Sox9*-lineage tracing also revealed the existence of a continuous cell supply from a *Sox9*-expressing population residing in the basal layers to the entire hyponychium epidermis. Furthermore, digit-tip regeneration is compromised in *Sox9*-knockout mice, revealing an essential role for the gene during this process. These results will contribute to understand the cellular and molecular basis of mammalian nail organ homeostasis and disease and digit-tip regeneration and will help to design new treatment strategies for patients with nail diseases or amputation.

Journal of Investigative Dermatology (2022) **142,** 2613–2622; doi:10.1016/j.jid.2022.03.020

INTRODUCTION

The nail organ is a specialized appendage at the end of the digits in which several ectodermal tissues function coordinately to sustain the continuous growth of the hard keratin nail plate. The nail matrix stands at the proximal base of the nail plate and is followed distally by the nail bed, which is a highly vascularized epithelium containing specialized ridges that attach the nail plate to the digit. There are two dedicated epidermal layers surrounding the nail, the eponychium in the proximal fold and the hyponychium in the distal one, which provide protection from injury and infection (Fleckman et al., 2013).

Two pools of nail stem cells responsible for the renewal and growth of the nail cell types have been described. The first one consists of slow-cycling label-retaining cells organized in a ring-like formation around the nail root, which under normal physiological conditions predominantly support the perinail epidermis, whereas during nail injury, they mostly contribute to the nail matrix and differentiated nail plate, showing their ability to adapt to wounding stimuli (Leung et al., 2014). The second stem cell population resides in the nail matrix and sustains nail growth. They are highly proliferative self-renewing nail stem cells that contribute to both the nail plate and the nail bed. In distal nail matrix cells, the Wnt signaling pathway is activated, and ablation of β-catenin, the intracellular mediator of this pathway, in the nail epithelium resulted in the cessation of stem cell differentiation so that the entire nail epithelium exhibited features of proximal matrix cells (Takeo et al., 2013).

The digit tips of mice and infant humans are capable of complete regeneration after amputation (Borgens, 1982; Illingworth, 1974). This is a multistep complex process in which both the nail organ and the terminal phalanx resume their preamputation organization. It starts with wound healing and re-epithelization of the amputated area. Subsequently, the blastema, a mesenchymal cell mass that differentiates into different cell types of the digit, is formed under the wound area. The formation and differentiation of the blastema is a key process in mammalian digit regeneration because failure to form it results in a lack of regeneration (Pulawska-Czub et al., 2021; Storer and Miller, 2020). Genetic lineage tracing showed that blastema cells are germ-layer restricted (Lehoczky et al., 2011; Rinkevich et al., 2011), and recent single-cell transcriptomic analyses have addressed the origin and differentiation potential of blastema progenitor cells (Johnson et al., 2020; Storer et al., 2020). The nail organ also plays a central role in digit regeneration by signaling the underlying blastema. Deletion of β-catenin in the nail epithelium after digit-tip amputation abrogated terminal phalanx regeneration (Takeo et al., 2013). Consistent with this, LGR6, an agonist of Wnt signaling, which is a marker for nail matrix stem cells, is also necessary for digit-tip regeneration (Lehoczky and Tabin, 2015).

The transcription factor SOX9 has multiple functions during the development and homeostasis of adult tissues (Jo et al., 2014). In this study, we have studied the role of *Sox9*

[1]*Laboratories 127 and a105, Department of Genetics and Biotechnology Institute, Center for Biomedical Research, University of Granada, Avenida del Conocimiento S/N, Armilla, Granada, Spain; and* [2]*Epigenetics and Sex Development Group, The Berlin Institute for Medical Systems Biology (BIMSB), Max Delbrück Center for Molecular Medicine, Berlin, Germany*

[3]*These authors contributed equally to this work.*

Correspondence: Francisco J. Barrionuevo, Laboratories 127 and a105, Department of Genetics and Biotechnology Institute, Center for Biomedical Research, University of Granada, Avenida del Conocimiento S/N, 18016 Armilla, Granada, Spain. E-mail: fjbarrio@go.ugr.es

Abbreviations: DAA, day after amputation; DATX, day after tamoxifen administration; K5, keratin 5; TCF1, T-cell factor 1

Received 15 December 2021; revised 15 March 2022; accepted 30 March 2022; accepted manuscript published online 7 April 2022; corrected proof published online 7 May 2022

during adult nail organ homeostasis and found that it is necessary for epithelial nail-bed cell differentiation and for maintenance of the underneath terminal phalanx. We also show that *Sox9* is essential for digit-tip regeneration.

RESULTS

Sox9 is expressed in various cell populations of the mouse digit tip

The expression of *Sox9* in the murine digit tip was assessed by immunofluorescence. We found $SOX9^+$ cells in the hair follicles, in the distal groove, in the proximal nail-fold epithelium, and in a wide region within the nail epithelium. In addition, we detected a weaker expression of *Sox9* in the basal layers of the hyponychium epidermis (Figure 1a–d). To better characterize the expression domain of $SOX9^+$ cells, we performed double immunofluorescence for SOX9 and three epidermal differentiation and proliferation markers (Figure 1e–k). In the digit tip, keratin 5 (K5), an epithelial marker (Fuchs, 2018), is expressed in the proximal fold, the nail matrix, the hyponychium, and the distal groove (Fleckman et al., 2013). SOX9 coexpressed with K5 in the proximal fold, the hyponychium, and the distal groove. In contrast, the proximal domain of SOX9 expression in the nail epithelium coincided with the distal $K5^+$ region (Figure 1e, f, and k). T-cell factor 1 (TCF1), a nuclear mediator of Wnt signaling, is expressed in the distal matrix within the nail epithelium (Takeo et al., 2013). We found that the proximal $SOX9^+$ region overlapped with the distal end of the TCF1-expression domain (Figure 1g, h, and k). According to Ki-67 expression in the nail epithelium, three differentiated regions are established: the highly proliferative proximal matrix, the low proliferative distal matrix, and the non-proliferative nail bed (Takeo et al., 2013). SOX9 expression was restricted to this latter region (Figure 1i, j, and k).

Lineage tracing of *Sox9*-expressing cells in the nail epithelium

The expression pattern of *Sox9* in the nail epithelium suggests that the gene is expressed in the nail bed, a region thought to be devoid of nail stem cells (Takeo et al., 2013). To test this hypothesis, we performed tamoxifen-inducible genetic lineage tracing using mice harboring an *IRES-CreER^{T2}* cassette inserted into the endogenous *Sox9* locus, *Sox9$^{IRES\text{-}CreERT2}$* (Soeda et al., 2010), and either an *R26R-LacZ* (Soriano, 1999) or an *R26R-EYFP* (Srinivas et al., 2001) allele. As expected, no LacZ- or EYFP-positive cells were detected at any of the stages analyzed in the absence of tamoxifen (not shown). We induced the labeling of *Sox9*-expressing cells and their progeny by tamoxifen administration to adult mice (aged 2 months) and analyzed the reporter expression on different days after tamoxifen administration (DATXs) (Figure 2a). Whole-mount analysis of cross-sectioned *Sox9$^{IRES\text{-}CreERT2}$;R26R-LacZ* digit tips 10 DATXs showed LacZ expression in both the nail-bed epithelium and the hyponychium (Figure 2b). Time-course analysis showed that the intensity of LacZ staining in the nail-bed epithelium increased between 1 and 10 DATXs (Figure 2c). This increasing number of labeled cells between 1 and 10 DATXs cannot be explained by cell proliferation because it is well known that nail-bed cells do not divide (Takeo et al., 2013; Zaias, 2014; results shown in this study). Rather, it is due to the fact that LacZ activity appears progressively in this tissue, occurring much more rapidly in some cells than in others. From 30 DATXs onward, LacZ staining was lost starting from the proximal-top region and proceeding to the distal-bottom region of the nail-bed epithelium. Forty-five DATXs, the nail bed showed almost no LacZ expression, and no staining was observed at later time points (Figure 2c and Supplementary Figure S1a). Accordingly, EYFP immunostaining of *Sox9$^{IRES-CreERT2}$;R26R-EYFP* digit sections showed that *Sox9*-expressing cells and their progeny were present in the entire nail-bed epithelium 10 DATXs but not 40 DATXs (Figure 2e–h and Supplementary Figure S1b, d, f, h, j, and l).

Continuous cell supply from *Sox9* progenitors to the hyponychium

As mentioned earlier, we also detected a population of $SOX9^+$ $K5^+$ cells in the distal groove and in the hyponychium (Figure 1e). *Sox9* lineage tracing between 3 and 10 DATXs revealed marked cells in the basal layer of the hyponychium. These cells were more frequently observed in the distal groove region (Figure 2i and k and Supplementary Figure S1c, e, g, and i). This latter observation is probably a consequence of tamoxifen reaching this region before the distal part of the hyponychium. Forty DATXs, the whole hyponychium showed strong EYFP staining, with $EYFP^+$ cells located in both the basal layers and the stratum corneum, indicating that *Sox9* progenitors terminally differentiate into skin corneocytes (Figure 2j and l and Supplementary Figure S1m). LacZ staining persisted even 1 year after tamoxifen administration (Supplementary Figure S1a).

Sox9 is required for epithelial nail-bed differentiation

To uncover new roles for *Sox9* in digit-tip homeostasis, we conditionally deleted the gene in adult mouse cells using a ubiquitous tamoxifen-inducible *CAGG-CreER^{TM}* recombinase (Hayashi and McMahon, 2002) (Figure 3a). Immunostaining revealed that SOX9 was efficiently removed from the nail epithelium of adult (aged ≥2 months) *CAGG-CreER^{TM};Sox9$^{flox/flox}$* (referred to as *Sox9$^{\Delta/\Delta}$* in the remaining part of this paper) mice 20 DATXs (Supplementary Figure S2a). Gross morphology analysis of the digit tip of *Sox9$^{\Delta/\Delta}$* mice 50 DATXs showed an outlandishly large claw-shaped fingernail (Figure 3b). Histology of mutant fingertips revealed that the hyponychium was absent and that the nail epithelium appeared to extend from the proximal fold directly to the distal groove. In contrast to that of the control mice, which presented a relatively thick nail matrix epithelium and a thinner nail bed, the mutant nail epithelium was very thick along its entire length. The longitudinal axis of the mutant nail plate was not oriented parallel to the nail epithelium, as observed in the control mice, but rather perpendicular to it and was much larger than that of the controls (Figure 3b and c and Supplementary Table S1). Time-course histological analysis of the phenotype of mutant digit tips revealed no apparent difference between them and controls 20 DATXs (not shown). In contrast, 30 DATXs, the mutant digit tip exhibited a clearly larger nail plate, and its nail epithelium experienced a thickening process extending throughout the former nail-bed domain. Forty DATXs, the thickened nail epithelium reached the distal groove, and the nail plate emerged along its entire length (Figure 3d–f). Marker analysis of the nail epithelium revealed that 30

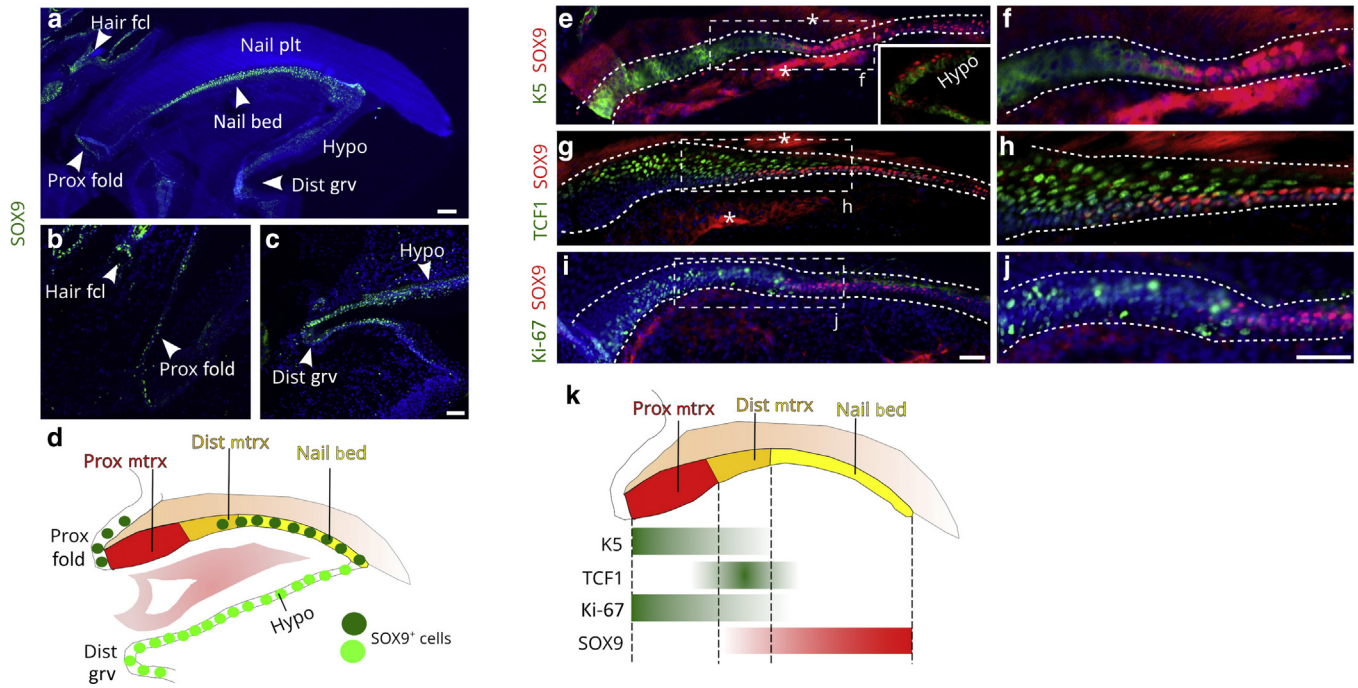

Figure 1. *Sox9* expression in the digit tip of adult mice. (**a**) Immunofluorescence for SOX9 in digit-tip sections of control mice and (**b**) high magnification of the Prox Fold and (**c**) Dist Grv and Hypo regions. (**d**) Schematic illustration of the digit-tip anatomy and *Sox9* expression pattern. Dark green circles indicate strong expression, and light green circles indicate weak expression. (**e–j**) Double immunofluorescence for SOX9 and either (**e, f**) K5 or (**g, h**) TCF1 or (**i, j**) Ki-67. Dashed lines outline the nail epithelium domain. Dashed rectangles in **e**, **g**, and **i** mark the areas shown at higher magnification in **f**, **h**, and **j**, respectively. (**k**) Schematic summary of this immunofluorescence analysis. Asterisks indicate areas of nonspecific, autofluorescent background. Bars shown in **a**, **c**, **i**, and **j** = 100 μm for **a**; 50 μm for **b** and **c**; 50 μm for **e**, **g**, and **i**; and 50 μm for **f**, **h**, and **j**, respectively. Dist Grv, distal groove; Dist Mtrx, distal matrix; Hair Fcl, hair follicle; Hypo, hyponychium; K5, keratin 5; Nail Plt, nail plate; Prox Fold, proximal fold; Prox Mtrx, proximal matrix; TCF1, T-cell factor 1.

DATXs, the expression of K5 was similar to that of controls. However, 40 DATXs, the expression domain of K5 was enlarged, and 50 DATXs, the entire nail epithelium was strongly K5 positive (Figure 3g–i and p and Supplementary Figure S2b). Similarly, 30 DATXs and afterward, the expression of *Tcf1* was not restricted to the distal nail matrix and extended along the entire length of the distal nail epithelium (Figure 3j–l and p and Supplementary Figure S2b). In addition, 30 DATXs and at later time points, the number of Ki-67^{+}cells was markedly increased in the mutants compared with that in the controls, and they occupied the entire length of the nail epithelium (Figure 3m–o and p). A well-known event in the process of nail keratinocyte cornification is the removal of the nucleus and the degradation of nuclear DNA (Jaeger et al., 2019). To identify the cells undergoing DNA fragmentation in the nail region, we performed a TUNEL assay. In control mice, TUNEL^{+} cells were located in the keratogenous zone, the region where nail matrix cells undergo terminal keratinocyte differentiation. However, in 40-DATX–mutant nails, the number of TUNEL^{+} cells was much higher and occupied the entire basal domain of the nail plate (Figure 3q), evidencing intense keratinocyte differentiation. Consistent with this, the expression of AE13, a marker for keratinized nail plate cells, revealed massive areas of keratinized nail plate tissue (Figure 3g–o and Supplementary Figure S2b). All these results show that in the mutant nail epithelium, the nail bed is absent, and the entire epithelium acquires the characteristics of nail matrix stem cells, which undergo active cell proliferation and follow the cornified nail plate cell fate.

Sox9 is necessary for the maintenance of the terminal phalanx

Histology of 50-DATX digit tips showed that the terminal phalanx of *Sox9*$^{\Delta/\Delta}$ mice was shorter, having a blunt distal tip with a pitted, irregular surface instead of the triangular sharp-pointed tip seen in control mice (Figure 3b). Whole-mount alizarin red staining revealed no remarkable differences between control and mutant terminal phalanxes 30 DATXs. In contrast, 40 DATXs, mutant mice presented terminal phalanxes with fragmented distal tips, and 50 DATXs, mutant terminal phalanxes were significantly shorter and lacked the whole distal tip (Figure 3r–t and Supplementary Table S1). To deepen the mechanisms responsible for this mutant bone regression, we performed a TUNEL assay and detected numerous apoptotic cells in the tip of the terminal phalanx. Contrarily, we found no apoptotic cells in the same region as that of the control mice (Figure 3u). We also examined the activity of tartrate-resistant acid phosphatase, a marker of osteoclastogenesis (Minkin, 1982). Control digit tips lacked tartrate-resistant acid phosphatase activity. Contrarily, the *Sox9*$^{\Delta/\Delta}$ terminal phalanx 40 DATXs showed a strong tartrate-resistant acid phosphatase signal in the distal tip area, indicating the presence of active osteoclasts and bone resorption (Figure 3v).

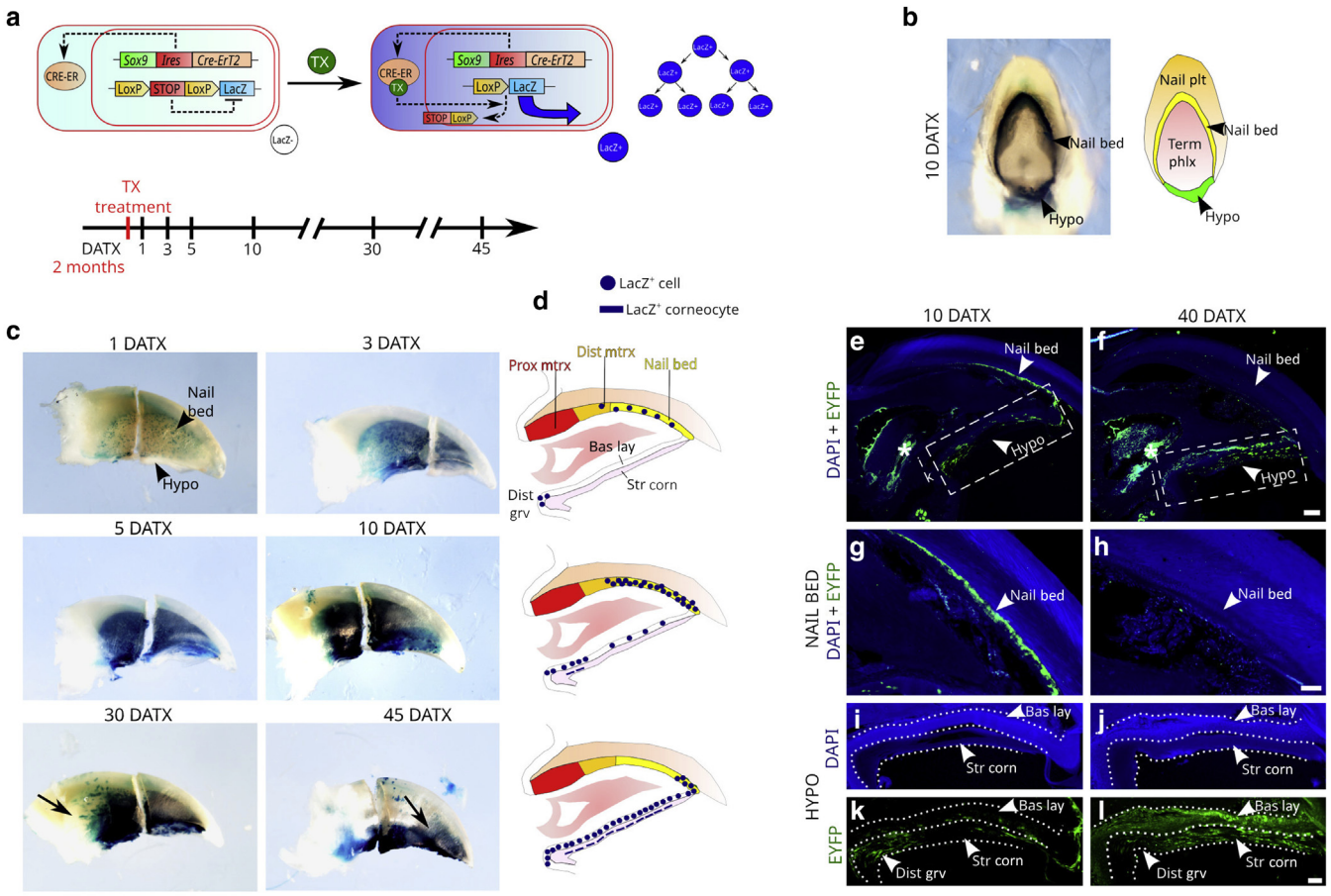

Figure 2. Lineage tracing of *Sox9*-expressing cells in the mouse digit tip. (**a**) Experimental strategy to trace the fate of *Sox9*-expressing cells using *Sox9*$^{IRES\text{-}CreERT2}$;*R26R-LacZ* mice. (**b**) Whole-mount LacZ staining of a cross-sectioned *Sox9*$^{IRES\text{-}CreERT2}$;*R26R-LacZ* digit tip 10 DATX and equivalent schematic illustration of the digit-tip anatomy. (**c**) Lateral view of whole-mount LacZ staining of *Sox9*$^{IRES\text{-}CreERT2}$;*R26R-LacZ* digit tips at the indicated DATXs. Arrows point to the proximal edge of the expression domain of LacZ^{+} cells in the nail bed. (**d**) Schematic illustrations of the digit tips shown in **c** (longitudinal sections), showing the fate of *Sox9*-expressing cells. (**e**–**l**) EYFP immunostaining of *Sox9*$^{IRES\text{-}CreERT2}$;*R26R-EYFP* digit longitudinal sections. Whole digit tip (**e**) 10 and (**f**) 40 DATXs. Dashed rectangles in **e** and **f** mark the area shown in **i** and **k** and **j** and **l**, respectively. (**g, h**) Higher magnification of the nail-bed region. Higher magnification of the Hypo epidermis showing (**i, j**) the blue (DAPI) and (**k, l**) the green (EYFP) channel. Asterisks indicate areas of nonspecific, autofluorescent background. Bars shown in **f**, **h**, and **l** = 100 μm for **e** and **f**, 50 μm for **g** and **h**, and 50 μm for **i**–**l**, respectively. Bas Lay, basal layer of the hyponychium epidermis; DATX, day after tamoxifen administration; Dist Grv, distal groove; Dist Mtrx, distal matrix; Hypo, hyponychium; Nail Plt, nail plate; Prox Mtrx, proximal matrix; Str Corn, stratum corneum of the hyponychium epidermis; Term Phlx, terminal phalanx; TX, tamoxifen.

Sox9 is necessary for digit regeneration

Next, we decided to address the role of *Sox9* during digit regeneration. For this, we treated *Sox9*-conditional mutant mice with tamoxifen starting immediately after digit-tip amputation (Figure 4a). Alizarin red staining of digits 50 days after amputation (DAAs) showed that the terminal phalanxes of control mice were triangular in shape with a sharp-pointed tip, whereas *Sox9*$^{\Delta/\Delta}$ phalanxes lacked its distal tip and were significantly shorter (Figure 4b and c and Supplementary Table S1). At the histological level, control and mutant amputated digits were indistinguishable 20 DAAs when the wounded area had already re-epithelialized in both cases. However, at later time points, the nail plate of the amputated *Sox9*$^{\Delta/\Delta}$ digits became larger, and the digit-bone length became smaller, and 50 DAAs, amputated *Sox9*$^{\Delta/\Delta}$ digits looked like nonamputated ones, without hyponychium, with terminal phalanxes lacking the distal tip, and with a nail epithelium extending from the proximal fold directly to the distal groove (Figure 4b and Supplementary Figure S3a). Similar to that in nonamputated *Sox9*$^{\Delta/\Delta}$ digits, this phenotype could be a consequence of the extended nail matrix domain. To test this hypothesis, we performed immunofluorescence for TCF1 and observed that the *Tcf1*-expression domain in the nail epithelium was extended distally in the mutants (Figure 4d and e). Consistent with this, the TUNEL assay showed that the keratogenous zone also extended distally in the amputated *Sox9*$^{\Delta/\Delta}$ digits (Figure 4f and g), and AE13 expression confirmed an increase in differentiated keratinized nail plate cells (Figure 4d and e). Next, we assessed osteoblast commitment in the underneath blastema by means of RUNX2 immunohistochemistry (Figure 4h). The number of RUNX2^{+} cells was reduced to a half in the *Sox9*$^{\Delta/\Delta}$ mesenchyme compared with that in the controls, indicating that osteoblast commitment is compromised in the absence of SOX9 (Figure 4i and Supplementary Table S1). We also studied apoptosis in the blastema and observed that TUNEL^{+}

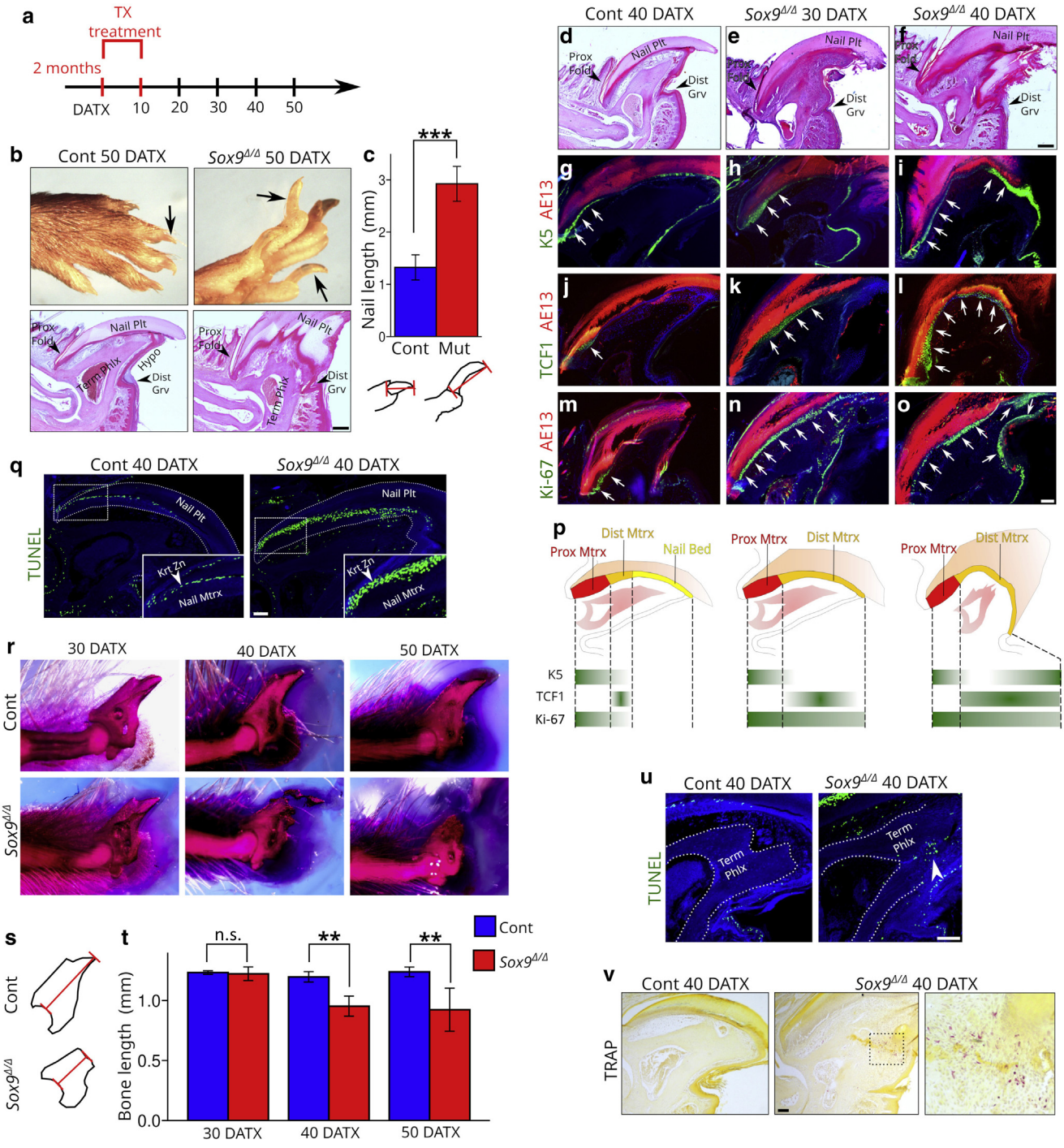

Figure 3. Digit phenotype of *Sox9*$^{\Delta/\Delta}$ adult mice. (**a**) Experimental schedule to study adult digit tips from mice with a conditional deletion of *Sox9*. (**b**) Gross morphology and histological sections of Cont and *Sox9*$^{\Delta/\Delta}$ toes 50 DATX. Arrows point to the Nail Plt. (**c**) Quantification analyses of the nail length at 50 DATX and schematic illustration of nail length measurement (the length of the red line was measured). (**d**–**f**) Histological sections of Cont and *Sox9*$^{\Delta/\Delta}$ digit tips at the indicated DATXs. (**g**–**o**) Double immunofluorescence for AE13 and either (**g**–**i**) K5, (**j**–**l**) TCF1, or (**m**–**o**) Ki-67 in Cont and *Sox9*$^{\Delta/\Delta}$ digit-tip sections at the same time point as in **d**–**f**. Arrows mark the extension of the different expression domains along the nail epithelium. (**p**) Graphical summary of the immunofluorescence analysis shown in **g**–**o.** (**q**) TUNEL staining of Cont and *Sox9*$^{\Delta/\Delta}$ digit tips 40 DATXs. Insets show higher magnifications of dashed areas. (**r**) Alizarin red staining of Cont and *Sox9*$^{\Delta/\Delta}$ digit tips at the indicated DATXs. (**s**) Schematic illustration of bone length measurement (the length of the red line was measured). (**t**) Quantification analyses of the bone length at the indicated time points. (**u**) TUNEL assay of the Term Phlx of Cont and *Sox9*-Muts digits. Dotted lines outline the section area occupied by the Term Phlx. (**v**) TRAP staining of Cont and *Sox9*$^{\Delta/\Delta}$ digit tips 40 DATXs. The right micrograph is a higher magnification of the square area outlined in the central micrograph. $^{**}P < 0.01$ and $^{***}P < 0.001$. Bars shown in **b**, **f**, **o**, **q**, **u**, and **v** = 200 μm for **b**, 200 μm for **d**–**f**, 100 μm for **g**–**o**, 100 μm for **q**, 50 μm for **u**, and 100 μm for **v**, respectively. Cont, control; DATX, day after tamoxifen administration; Dist Grv, distal groove; Dist Mtrx, distal matrix; Hypo, hyponychium; K5, keratin 5; Krt Zn, keratogenous zone; Mut, mutant; Nail Mtrx, nail matrix; Nail Plt, nail plate; n.s., not significant; Prox Fold, proximal fold; Prox Mtrx, proximal matrix; Term Phlx, terminal phalanx; TCF1, T-cell factor 1; TRAP, tartrate-resistant acid phosphatase; TX, tamoxifen.

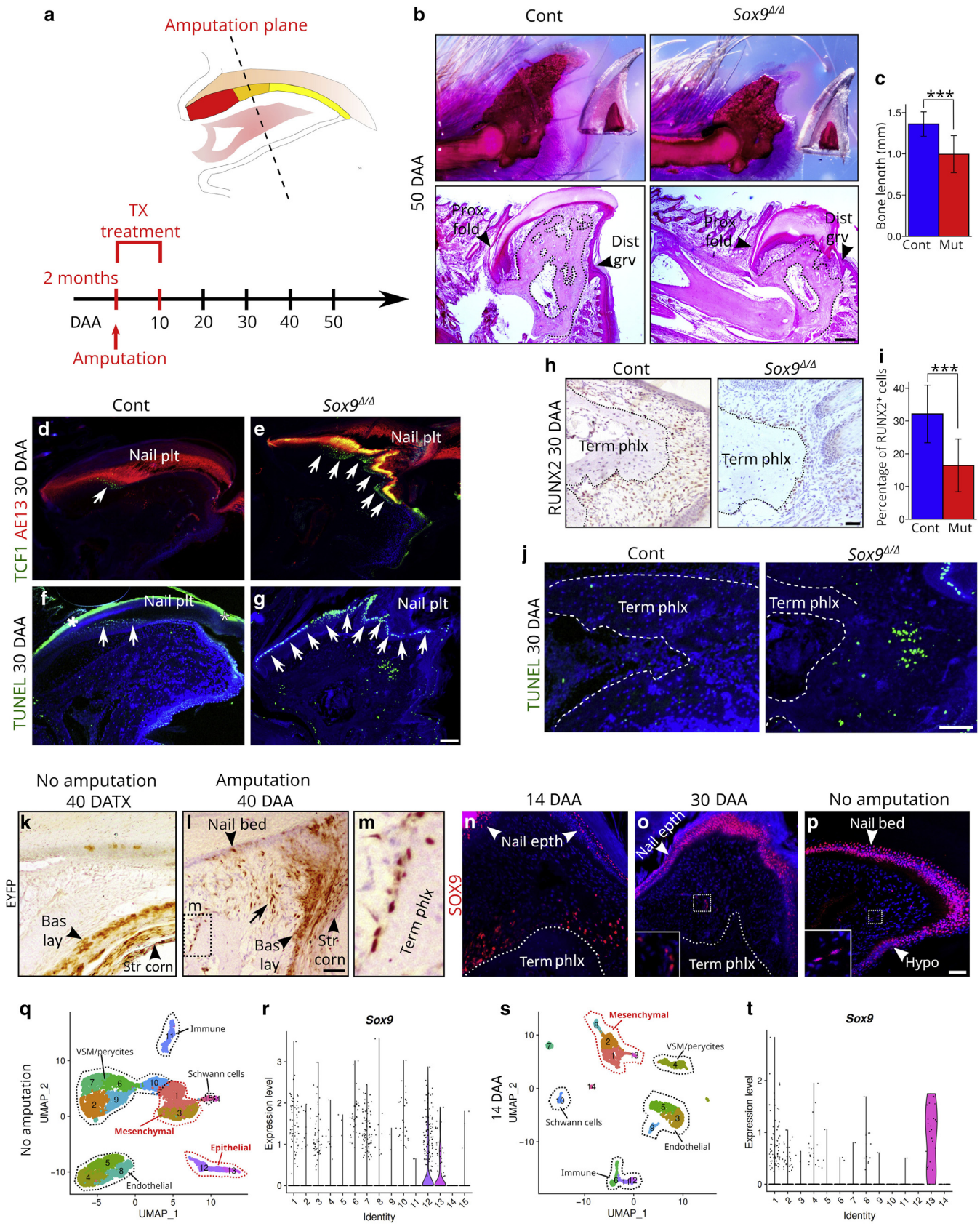

Figure 4. Role of *Sox9* in mouse digit regeneration. (**a**) Experimental strategy for digit-tip regeneration analysis. (**b**) Alizarin red staining and histology of amputated Cont and *Sox9*$^{\Delta/\Delta}$ digit tips 50 DAAs. Dotted lines outline the section area occupied by the Term Phlx. (**c**) Quantification analyses of the bone length 50 DAAs. (**d, e**) Double immunofluorescence for AE13 and TCF1 in amputated Cont and *Sox9*$^{\Delta/\Delta}$ digit tips 30 DAAs. Arrows mark the extension of the TCF1 expression domain. (**f, g**) TUNEL staining of amputated Cont and *Sox9*$^{\Delta/\Delta}$ digit tips 30 DAAs. Arrows mark the extension of the area occupied by apoptotic cells. (**h**) Immunohistochemistry for RUNX2 in amputated Cont and *Sox9*$^{\Delta/\Delta}$ digit tips 30 DAAs. (**i**) Quantification of the number of RUNX2^{+} cells in the blastema.

cells accumulated in the region distal to the terminal phalanx of $Sox9^{\Delta/\Delta}$ mice but not in the same region as that in the control mice (Figure 4j).

To trace the fate of *Sox9*-expressing cells during digit regeneration, we treated *Sox9-IRES-CreERT2;R26R-EYFP* mice with tamoxifen starting on the day of amputation. Forty DAAs, we observed $EYFP^+$ cells in the nail-bed epithelium as well as in the basal layers and the stratum corneum of the hyponychium, as previously shown for nonamputated digits. However, unlike that in the nonamputated digits, we also found $EYFP^+$ cells in the mesenchyme underneath the nail epithelium of amputated digits (Figure 4k and l). It is unlikely that the progenitors of these $EYFP^+$ cells reside in either the nail bed or the hyponychium because it is widely accepted that during digit regeneration, progenitor cells are fate restricted (Lehoczky et al., 2011; Rinkevich et al., 2011). Because of this, we studied the expression of *Sox9* during digit-tip regeneration and found $SOX9^+$ cells in the nail epithelium at all the stages analyzed. We also observed many $SOX9^+$ cells in the blastema of amputated digits before 20 DAAs but not 30 DAAs and at posterior stages, when $SOX9^+$ cells were rarely observed in the mesenchyme underlying the nail epithelium, as observed in nonamputated digits (Figure 4n–p and Supplementary Figure S3b). These findings indicate that *Sox9* may have two roles during digit regeneration: one in blastema cells and another one in epithelial cells. Therefore, we used the single-cell RNA-sequencing datasets recently generated by Storer et al. (2020) during digit regeneration at different DAAs. Unbiased clustering of 10, 14, and 28 DAAs and nonamputated digit-tip datasets and subsequent assignation of cell identity (see dot plots in Supplementary Figure S3c) revealed the cell populations equivalent to those identified by Storer et al. (2020) (Figure 4q and s and Supplementary Figure S3d and f), although the actual number of clusters may vary depending on the sensitivity chosen in the clustering algorithm. Consistent with our immunohistology, cluster marker identification and violin plots revealed that all epithelial clusters were enriched in $Sox9^+$ cells, as was a mesenchymal cluster both 10 DAAs (cluster 9) and 14 DAAs (cluster 13) but not 28 DAAs or in the nonamputated digits (Figure 4r and t and Supplementary Figure S3e and g and Supplementary Tables S2–5). To investigate the role of *Sox9* during blastema differentiation, we used the transcriptomic signature of the identified mesenchymal clusters (clusters 1, 2, 8, and 13) 14 DAAs (Supplementary Table S4) and compared the resulting enriched biological processes in a Gene Ontology analysis. We observed that all these clusters showed enriched terms related to cartilage and bone development. In addition, one cluster (cluster 8) was also enriched in categories associated with cell division (Supplementary Figure S3h and Supplementary Table S6). Gene Ontology analysis is not effective to distinguish among related categories because they share many genes. Thus, we looked for differentially expressed genes between the $Sox9^+$ mesenchymal cluster (cluster 13) and the other mesenchymal clusters (clusters 1, 2, and 8) (Supplementary Table S7), and Gene Ontology enrichment analysis using the upregulated genes in cluster 13 revealed the terms associated to extracellular matrix organization and cartilage development (Supplementary Figure S3i and Supplementary Table S8). During endochondral bone differentiation, *Sox9* is expressed in mesenchymal chondroprogenitors, where it is required for chondrocyte differentiation and for the deposition of extracellular matrix proteins. Subsequently, *Sox9* is downregulated as hypertrophic chondrocytes undergo osteoblast differentiation (Akiyama et al., 2002; Bi et al., 1999; Ng et al., 1997; Zhao et al., 1997). Consistent with this, we found genes encoding chondrocyte extracellular matrix proteins that were specifically or preferentially expressed in the $Sox9^+$ mesenchymal cluster, including *Col2a1, Col11a2, Col9a1*, and *Acan*, which are known to be directly regulated by SOX9 (Supplementary Figure S3j and Supplementary Table S4) (Bell et al., 1997; Bridgewater et al., 1998; Sekiya et al., 2000; Zhang et al., 2003). We also looked for key markers of osteoblast differentiation (Komori, 2018, 2006) and found a set of genes that were preferentially expressed in the mesenchymal *Sox9*-negative clusters (Supplementary Figure S3k and Supplementary Table S4). These results are consistent with the hypothesis that $Sox9^+$ mesenchymal cells present in the blastema initiate a chondrogenic-like process and subsequently undergo osteoblast differentiation. Accordingly, we observed *Sox9*-descendant cells on the surface of the terminal phalanxes of lineage tracer mice 40 DAAs (Figure 4m).

As mentioned, *Sox9* was expressed in all the epithelial clusters identified in our analysis. Because of this, in this case, we used the results of the analysis of the combined 11, 12, 14, and 17 DAAs and nonamputated single-cell RNA-sequencing datasets recently generated by Johnson et al. (2020). These authors identified three epithelial clusters, and in one of them, *Sox9* was not present in the transcriptomic signature (see Supplementary Table S3 in the study by Johnson et al. [2020]). We compared the enriched biological processes using the transcriptomic signature of these three clusters and found that only the *Sox9*-negative cluster was enriched in terms related to cell proliferation, the others being significantly enriched in categories associated with

***$P < 0.001$. (**j**) TUNEL staining of amputated Cont and $Sox9^{\Delta/\Delta}$ phalanx tips 30 DAAs. (**k–m**) EYFP immunohistochemistry on sections of (**k**) nonamputated and (**m**) amputated *Sox9*$^{IRES\text{-}CreERT2}$*;R26R-EYFP* digit tips at the indicated time points. Arrows point to EYFP-positive cells in the mesenchyme. The dotted rectangle in **l** marks the area shown at higher magnification in **m**. (**n–p**) Immunofluorescence for SOX9 in (**n, o**) amputated and (**p**) nonamputated Cont digit tips at the indicated time points. The dotted squares mark the area shown at higher magnification in the insets. (**q, s**) UMAP visualization of cell clusters identified in the scRNA-seq analysis of (**q**) nonamputated and (**s**) amputated digit tips 14 DAAs. (**r, t**) Violin plot showing *Sox9* expression in clusters identified in (**r**) nonamputated and (**t**) amputated digit tips 14 DAAs. Bars shown in **b**, **g**, **h**, **j**, **l**, and **p** = 200 μm for **b**, 100 μm for **d–g**, 50 μm for **h**, 50 μm for **j**, 50 μm for **k** and **l,** and 50 μm for **n–p**, respectively. Bas Lay, basal layer; Cont, control; DAA, day after amputation; DATX, day after tamoxifen administration; Dist Grv, distal groove; Nail Epth, nail epithelium; Nail Plt, nail plate; Prox Fold, proximal fold; scRNA-seq, single-cell RNA sequencing; Str Corn, stratum corneum; TCF1, T-cell factor 1; Term Phlx, terminal phalanx; TX, tamoxifen; UMAP, Uniform Manifold Approximation and Projection.

ribosome biogenesis (Supplementary Figure S3I and Supplementary Table S9).

DISCUSSION

In this study, we have identified a population of *Sox9*-expressing cells in the basal layer of the distal groove and the hyponychium, and using lineage tracing experiments, we have shown that they are involved in the homeostasis of the hyponychium epidermis. During mouse embryonic and postnatal skin development, *Sox9* is initially expressed in the hair placodes, and subsequently, its expression persists in the upper outer root sheath, where it overlaps with quiescent H2B–GFP label–retaining cells that give rise to the adult bulge (Nowak et al., 2008; Vidal et al., 2005). Consistent with this, *Sox9*-lineage tracing during hair follicle development showed that under normal physiological conditions, *Sox9*-descendant cells contribute to the entire hair follicle but not to the interfollicular epidermis (Nowak et al., 2008). The situation in the nail organ seems to be different because in this study, we report that descendants of *Sox9*-expressing cells from the basal layers of the hyponychium contribute to the entire epidermis. We detected $LacZ^+$ cells even 1 year after tamoxifen administration, indicating that these *Sox9*-expressing cells function as self-renewing adult stem cells that continuously sustain the entire hyponychium epidermis. Therefore, our results suggest that in contrast to the role observed in the interfollicular epidermis, *Sox9* may have a role in epidermal stem cell maintenance and/or differentiation in the hyponychium.

We found another *Sox9*-expressing cell population in the nail-bed epithelium, as observed in previous expression studies using human tissue (Krahl and Sellheyer, 2010). We have shown that *Sox9* functions in the nail-bed epithelium as a master regulatory gene essential for the differentiation of nail-bed cells. Our results revealed that *Sox9* upregulation in the nail epithelium coincides with (i) the downregulation of the Wnt signaling pathway; (ii) a decrease in cell proliferation; and (iii) an increase in ribosome biogenesis, a biological process that has been associated with stem cell differentiation (Brombin et al., 2015; Sanchez et al., 2016). Thus, taking into consideration these results and the fact that SOX9 is a known antagonist of Wnt signaling (Akiyama et al., 2004; Kim et al., 2006; Sinha et al., 2021), it is conceivable that during nail-bed differentiation, SOX9 represses Wnt signaling, leading to altered biological processes such as reduced cell proliferation and increased ribosome biogenesis.

Sox9-driven cell lineage tracing showed that mouse epithelial nail-bed cells are completely replaced in about 30 days and that they do not contribute neither to the nail plate nor to the underlying mesenchyme under normal physiological conditions, as reported in previous studies (Takeo et al., 2013; Zaias and Alvarez, 1968). Despite the large number of studies carried out on the nail organ, the role of the nail bed during nail homeostasis has remained unclear, being considered an epithelium whose main function is just to keep the nail attached to the underlying digit (Zaias, 2014). Our analysis of $Sox9^{\Delta/\Delta}$ digit tips, in which the nail-bed epithelium is absent, clearly provides evidence that this cell population has additional functions. First, we have shown that the nail bed is necessary to maintain the normal physiological growth of the nail plate. If nail-bed cells are not present, the distal nail matrix ($K5^+$ $TCF1^+$) expands distally, generating an elongated highly proliferative epithelium that undergoes keratinocyte differentiation, and as a consequence, a large claw-shaped fingernail arises that grows perpendicular to the nail epithelium. Second, our results also indicate that the nail bed is necessary for the maintenance of the underlying digit bone. In *Sox9* mutants, the terminal phalanx undergoes both bone reabsorption and apoptosis, and the distal tip is finally lost. A similar phenotype was observed when Wnt signaling was deleted from the nail epithelium (Takeo et al., 2016, 2013). In this case, a lack of Wnt activation in osteoblast and osteoclast precursors was reported, leading to the regression of the underneath terminal phalanx (Takeo et al., 2016). In our *Sox9* mutants, Wnt signaling in the nail epithelium is apparently active, as shown by *Tcf1* expression. However, osteoclast precursors are also active, indicating that nail-bed cells may act as signaling centers necessary for the homeostatic maintenance of the underlying digit-tip bone.

We have also studied the role of *Sox9* during digit-bone regeneration. In the absence of SOX9, the distal tip of the terminal phalanx does not regenerate after amputation, leading to a phenotype similar to that of nonamputated $Sox9^{\Delta/\Delta}$ digit tips. Our results indicate that two events can contribute to this phenotype. First, as observed in nonamputated digit tips, epithelial nail-bed cells do not differentiate in amputated digits lacking SOX9, and the nail matrix expands distally. Takeo et al. (2013) reported that the nail epithelial function is necessary for digit-tip regeneration. They inactivated Wnt signaling in the nail epithelium, and as a consequence, osteoblast commitment in blastema cells was compromised (Takeo et al., 2013). In this study, we show that osteoblast commitment is also compromised in the blastema of *Sox9* mutants, indicating that signaling from the nail bed is also necessary for digit regeneration. Second, we have observed descendants of *Sox9*-expressing cells in the blastema of amputated digits, which were not present in nonamputated digits. A possible explanation for the origin of these cells is that either nail bed or hyponychium cells undergo an epithelial-to-mesenchymal transition during the course of digit regeneration. However, this is unlikely to occur because several studies using genetic lineage tracing (Lehoczky et al., 2011; Rinkevich et al., 2011) and single-cell transcriptomic profiling (Johnson et al., 2020; Storer et al., 2020) have shown that progenitor cells of the digit blastema are germ-layer restricted. An alternative explanation is that *Sox9* is upregulated in a population of blastema cells during digit regeneration. We have shown by both immunofluorescence and single-cell profiling that this indeed is the case. Our results indicate that SOX9 may control the early steps of blastema–mesenchyme cell differentiation into osteoblasts, as normally occurs during endochondral bone differentiation (Akiyama et al., 2002; Bi et al., 1999). This implies that mesenchymal cells undergo a process of endochondral-like osteoblast differentiation in amputated digits, which contrasts with the findings of previous studies indicating that bone regeneration after digit-tip amputation occurs by direct ossification (Han et al., 2008; Muller et al., 1999). Two different situations could explain this apparent

discrepancy. The first one is that both mechanisms do operate in parallel during digit-tip regeneration. The second one is that the process of osteoblast differentiation only partially recapitulates the mechanisms known to be active during development, which is supported by the observation that blastema cells express mesenchyme developmental genes but do not acquire an embryonic digit state (Storer et al., 2020). In conclusion, we have shown that *Sox9* is essential for digit-tip regeneration, and our results indicate that two *Sox9*-expressing cell populations exist that can contribute to this process: one in the nail epithelium and another one in the differentiating blastema. The conditional deletion of the gene specifically in epithelial cells (e.g., using a *K14-CreER* mouse line) and in blastema cells (e.g., using a *Pdgfra-CreER* mouse line) would help to elucidate the contribution of both cell populations to this process.

In summary, in this study, we show that SOX9 is necessary for both nail organ homeostasis and digit regeneration. This knowledge will provide insights into the genetic basis of nail diseases, whose etiology remains unknown, and the mechanism governing mammalian digit-tip regeneration, which can contribute to developing new therapies for patients with nail disease or amputation.

MATERIALS AND METHODS

Mice and crosses

For genetic lineage tracing, *Sox9*$^{IRES\text{-}CreERT2}$ (*B6.129S7-Sox9*$^{tm1(cre/ERT2)Haak}$) mice (Soeda et al., 2010) were obtained from the RIKEN BioResource Research Center (Tsukuba, Japan). *R26R-LacZ* (*B6.129S4-Gt(ROSA)26Sor*$^{tm1Sor/J}$) (Soriano, 1999) and *R26R-EYFP* (*B6.129X1-Gt(ROSA)26Sort*$^{m1(EYFP)Cos/J}$) (Srinivas et al., 2001) mice were obtained from The Jackson Laboratory (Bar Harbor, ME). See Supplementary Materials and Methods for mouse crosses and tamoxifen administration protocols. Mouse housing and handling as well as laboratory protocols were approved by The University of Granada (Granada, Spain) Ethics Committee for Animal Experimentation (reference 12/12/2016/177).

Histological and immunohistological methods

A detailed explanation of the analysis of histology, immunohistology, digit-tip regeneration assays, morphometric analyses of terminal phalanxes and nails, alizarin red staining of bones, tartrate-resistant acid phosphatase staining, and analysis of apoptosis protocols is provided in Supplementary Materials and Methods.

Single-cell RNA-sequencing data analysis

We used the single-cell RNA-sequencing datasets from uninjured and amputated digits 10, 14, and 28 DAAs reported by Storer and Miller, 2020 (Gene Expression Omnibus GSE135985), and they were analyzed as detailed in Supplementary Materials and Methods.

Data availability statement

Datasets related to this article can be found at https://www.ncbi.nlm.nih.gov/geo/query/acc.cgi?acc=GSE135985, hosted at the Gene Expression Omnibus database repository (https://www.ncbi.nlm.nih.gov/geo/) and in https://docs.google.com/viewer?url=https%3A%2F%2Fars.els-cdn.com%2Fcontent%2Fimage%2F1-s2.0-S1534580700300587-mmc3.xlsx, corresponding to Supplementary Table S3 of the study by Johnson et al. (2020).

ORCIDs

Miguel Lao: http://orcid.org/0000-0001-6707-6825
Alicia Hurtado: http://orcid.org/0000-0001-6267-704X
Alejandro Chacón de Castro: http://orcid.org/0000-0003-0497-469X
Miguel Burgos: http://orcid.org/0000-0003-4446-9313
Rafael Jiménez: http://orcid.org/0000-0003-4103-8219
Francisco J. Barrionuevo: http://orcid.org/0000-0003-2651-1530

CONFLICT OF INTEREST

The authors state no conflict of interest.

ACKNOWLEDGMENTS

This work was supported by grants from the Andalusian Government, Junta de Andalucía, and BIO-109 to RJ and P11-CVI-7291 to MB and grants from the Spanish Ministry of Science and Innovation (CGL2011-23368 and CGL2015-67108-P) to RJ and FJB. The authors would like to thank the Spanish Ministry of Science and Innovation for the FPI PhD fellowship granted to ML and the FPU PhD fellowship granted to AH.

AUTHOR CONTRIBUTIONS

Conceptualization: RJ, FJB; Funding Acquisition: RJ, MB, FJB; Investigation: ML, AH, ACdC, MB, RJ, FJB; Visualization: FJB; Writing - Original Draft Preparation: RJ, FJB; Writing - Review and Editing: ML, AH, ACdC, MB, RJ, FJB

SUPPLEMENTARY MATERIAL

Supplementary material is linked to the online version of the paper at www.jidonline.org, and at https://doi.org/10.1016/j.jid.2022.03.020.

REFERENCES

Akiyama H, Chaboissier MC, Martin JF, Schedl A, de Crombrugghe B. The transcription factor Sox9 has essential roles in successive steps of the chondrocyte differentiation pathway and is required for expression of Sox5 and Sox6. Genes Dev 2002;16:2813–28.

Akiyama H, Lyons JP, Mori-Akiyama Y, Yang X, Zhang R, Zhang Z, et al. Interactions between Sox9 and beta-catenin control chondrocyte differentiation. Genes Dev 2004;18:1072–87.

Bell DM, Leung KK, Wheatley SC, Ng LJ, Zhou S, Ling KW, et al. SOX9 directly regulates the type-II collagen gene. Nat Genet 1997;16:174–8.

Bi W, Deng JM, Zhang Z, Behringer RR, de Crombrugghe B. Sox9 is required for cartilage formation. Nat Genet 1999;22:85–9.

Borgens RB. Mice regrow the tips of their foretoes. Science 1982;217:747–50.

Bridgewater LC, Lefebvre V. Crombrugghe B de. Chondrocyte-specific enhancer elements in the Col11a2 gene resemble the Col2a1 tissue-specific enhancer. J Biol Chem 1998;273:14998–5006.

Brombin A, Joly JS, Jamen F. New tricks for an old dog: ribosome biogenesis contributes to stem cell homeostasis. Curr Opin Genet Dev 2015;34:61–70.

Fleckman P, Jaeger K, Silva KA, Sundberg JP. Comparative anatomy of mouse and human nail units. Anat Rec (Hoboken) 2013;296:521–32.

Fuchs E. Skin stem cells in silence, action, and cancer. Stem Cell Reports 2018;10:1432–8.

Han M, Yang X, Lee J, Allan CH, Muneoka K. Development and regeneration of the neonatal digit tip in mice. Dev Biol 2008;315:125–35.

Hayashi S, McMahon AP. Efficient recombination in diverse tissues by a tamoxifen-inducible form of Cre: a tool for temporally regulated gene activation/inactivation in the mouse. Dev Biol 2002;244:305–18.

Illingworth CM. Trapped fingers and amputated finger tips in children. J Pediatr Surg 1974;9:853–8.

Jaeger K, Sukseree S, Zhong S, Phinney BS, Mlitz V, Buchberger M, et al. Cornification of nail keratinocytes requires autophagy for bulk degradation of intracellular proteins while sparing components of the cytoskeleton. Apoptosis 2019;24:62–73.

Jo A, Denduluri S, Zhang B, Wang Z, Yin L, Yan Z, et al. The versatile functions of Sox9 in development, stem cells, and human diseases. Genes Dis 2014;1:149–61.

Johnson GL, Masias EJ, Lehoczky JA. Cellular heterogeneity and lineage restriction during mouse digit tip regeneration at single-cell resolution. Dev Cell 2020;52:525–40.e5.

Kim Y, Kobayashi A, Sekido R, DiNapoli L, Brennan J, Chaboissier MC, et al. Fgf9 and Wnt4 act as antagonistic signals to regulate mammalian sex determination. PLoS Biol 2006;4:e187.

Komori T. Regulation of osteoblast differentiation by transcription factors. J Cell Biochem 2006;99:1233–9.

Komori T. Runx2, an inducer of osteoblast and chondrocyte differentiation. Histochem Cell Biol 2018;149:313–23.

Krahl D, Sellheyer K. Sox9, more than a marker of the outer root sheath: spatiotemporal expression pattern during human cutaneous embryogenesis. J Cutan Pathol 2010;37:350–6.

Lehoczky JA, Robert B, Tabin CJ. Mouse digit tip regeneration is mediated by fate-restricted progenitor cells. Proc Natl Acad Sci USA 2011;108:20609–14.

Lehoczky JA, Tabin CJ. Lgr6 marks nail stem cells and is required for digit tip regeneration. Proc Natl Acad Sci USA 2015;112:13249–54.

Leung Y, Kandyba E, Chen YB, Ruffins S, Chuong CM, Kobielak K. Bifunctional ectodermal stem cells around the nail display dual fate homeostasis and adaptive wounding response toward nail regeneration. Proc Natl Acad Sci USA 2014;111:15114–9.

Minkin C. Bone acid phosphatase: tartrate-resistant acid phosphatase as a marker of osteoclast function. Calcif Tissue Int 1982;34:285–90.

Muller TL, Ngo-Muller V, Reginelli A, Taylor G, Anderson R, Muneoka K. Regeneration in higher vertebrates: limb buds and digit tips. Semin Cell Dev Biol 1999;10:405–13.

Ng LJ, Wheatley S, Muscat GEO, Conway-Campbell J, Bowles J, Wright E, et al. SOX9 binds DNA, activates transcription, and Coexpresses with type II collagen during chondrogenesis in the mouse. Dev Biol 1997;183:108–21.

Nowak JA, Polak L, Pasolli HA, Fuchs E. Hair follicle stem cells are specified and function in early skin morphogenesis. Cell Stem Cell 2008;3:33–43.

Pulawska-Czub A, Pieczonka TD, Mazurek P, Kobielak K. The potential of nail mini-organ stem cells in skin, nail and digit tips regeneration. Int J Mol Sci 2021;22:2864.

Rinkevich Y, Lindau P, Ueno H, Longaker MT, Weissman IL. Germ-layer and lineage-restricted stem/progenitors regenerate the mouse digit tip. Nature 2011;476:409–13.

Sanchez CG, Teixeira FK, Czech B, Preall JB, Zamparini AL, Seifert JRK, et al. Regulation of ribosome biogenesis and protein synthesis controls germline stem cell differentiation. Cell Stem Cell 2016;18:276–90.

Sekiya I, Tsuji K, Koopman P, Watanabe H, Yamada Y, Shinomiya K, et al. SOX9 enhances aggrecan gene promoter/enhancer activity and is up-regulated by retinoic acid in a cartilage-derived cell line, TC6. J Biol Chem 2000;275:10738–44.

Sinha A, Fan VB, Ramakrishnan AB, Engelhardt N, Kennell J, Cadigan KM. Repression of Wnt/β-catenin signaling by SOX9 and mastermind-like transcriptional coactivator 2. Sci Adv 2021;7: *eabe*0849.

Soeda T, Deng JM. Crombrugghe B de, Behringer RR, Nakamura T, Akiyama H. Sox9-expressing precursors are the cellular origin of the cruciate ligament of the knee joint and the limb tendons. Genesis 2010;48:635–44.

Soriano P. Generalized lacZ expression with the ROSA26 Cre reporter strain. Nat Genet 1999;21:70–1.

Srinivas S, Watanabe T, Lin CS, William CM, Tanabe Y, Jessell TM, et al. Cre reporter strains produced by targeted insertion of EYFP and ECFP into the ROSA26 locus. BMC Dev Biol 2001;1:4.

Storer MA, Mahmud N, Karamboulas K, Borrett MJ, Yuzwa SA, Gont A, et al. Acquisition of a unique mesenchymal precursor-like blastema state underlies successful adult mammalian digit tip regeneration. Dev Cell 2020;52:509–24.e9.

Storer MA, Miller FD. Cellular and molecular mechanisms that regulate mammalian digit tip regeneration. Open Biol 2020;10:200194.

Takeo M, Chou WC, Sun Q, Lee W, Rabbani P, Loomis C, et al. Wnt activation in nail epithelium couples nail growth to digit regeneration. Nature 2013;499:228–32.

Takeo M, Hale CS, Ito M. Epithelium-derived Wnt ligands are essential for maintenance of underlying digit bone. J Invest Dermatol 2016;136:1355–63.

Vidal VPI, Chaboissier M-C, Lützkendorf S, Cotsarelis G, Mill P, Hui C-C, et al. Sox9 is essential for outer root sheath differentiation and the formation of the hair stem cell compartment. Curr Biol 2005;15:1340–51.

Zaias N. The nail bed, part I. The normal nail bed matrix, stem cells, distal motion and anatomy. J Dermatolog Clin Res 2014;2:1008.

Zaias N, Alvarez J. The formation of the primate nail plate. An autoradiographic study in squirrel monkey. J Invest Dermatol 1968;51:120–36.

Zhang P, Jimenez SA, Stokes DG. Regulation of human COL9A1 gene expression. Activation of the proximal promoter region by SOX9. J Biol Chem 2003;278:117–23.

Zhao Q, Eberspaecher H, Lefebvre V, de Crombrugghe B. Parallel expression of Sox9 and Col2a1 in cells undergoing chondrogenesis. Dev Dyn 1997;209:377–86.

SUPPLEMENTARY MATERIALS AND METHODS

Mice and crosses

For genetic lineage tracing, *Sox9*$^{IRES\text{-}CreERT2}$ (*B6.129S7-Sox9*$^{tm1(cre/ERT2)Haak}$) (Soeda et al., 2010) mice were obtained from the RIKEN BioResource Research Center (Tsukuba, Japan). *R26R-LacZ* (*B6.129S4-Gt(ROSA)26Sor*$^{tm1\text{-}Sor/J}$) (Soriano, 1999) and *R26R-EYFP* (*B6.129X1-Gt(ROSA)26Sort*$^{m1(EYFP)Cos/J}$) (Srinivas et al., 2001) mice were obtained from The Jackson Laboratory (Bar Harbor, ME). *Sox9*$^{IRES\text{-}CreERT2}$ mice were crossed to either *R26R-LacZ* or *R26R-EYFP* to generate double heterozygotes. To conditionally delete *Sox9*, *Sox9*$^{flox/flox}$ (*B6.129S7-Sox9*$^{tm2Crm/J}$) (Akiyama et al., 2002) and *CAGG-CreER*^{TM} (Hayashi and McMahon, 2002) (*B6.Cg-Tg(CAG-cre/Esr1*)*^{5Amc}) mice were acquired from The Jackson Laboratory. Both mouse strains were bred, and the resulting double heterozygous offspring was backcrossed to *Sox9*$^{flox/flox}$ mice to obtain *CAGG-CreER*^{TM}*;Sox9*$^{flox/flox}$ mice.

Tamoxifen administration

CAGG-CreER^{TM}*;Sox9*$^{flox/flox}$ mice were fed for 10 days with a diet (Harlan 2914 diet) supplemented with tamoxifen (40 mg tamoxifen/100 g diet; T5648, Sigma-Aldrich, St. Louis, MO). *Sox9* lineage-tracing mice were treated the same way as if they were to be analyzed 20 days after tamoxifen administration or later. For mice to be analyzed 20 days after tamoxifen administration, tamoxifen was dissolved in corn oil (C8267, Sigma-Aldrich) at a concentration of 30 mg/ml, and 0.2 mg of tamoxifen per gram of body weight was administered by a single intraperitoneal injection.

Histological and immunohistological methods

Digit tips were dissected out, fixed in 4% paraformaldehyde, decalcified in 10% EDTA in PBS for 30 days, dehydrated, embedded in paraffin, sectioned, and stained with H&E. Single and double immunofluorescence were performed as previously described (Dadhich et al., 2013). The three central rear paw digits were used for all the experiments. We found no differences either at the histological level or in the expression pattern of all markers analyzed between control digits without tamoxifen administration and control digits treated with tamoxifen at any time point (days after tamoxifen administration). The following antibodies were used: mouse anti-SOX9 (1/50; AMAB90795, Sigma-Aldrich), rabbit anti-SOX9 (1/400; AB5535, MilliporeSigma, Burlington, MA), rabbit anti–T-cell factor 1 (1/100; C63D9, Cell Signaling Technology, Danvers, MA), rabbit anti–Ki-67 (1/50; Ab15580, Abcam, Cambridge, United Kingdom), mouse anti-AE13 (1/100; Ab16113, Abcam), rabbit anti-GFP (1/100; NB600-308, Novus Biologicals, Littleton, CO), rabbit anti–keratin 5 (1/2,000; Ab52635, Abcam), and rabbit anti-RUNX2 (1/75; Ab23981, Abcam).

Digit-tip regeneration assays

For digit regeneration assays, mice aged ≥2 months were anesthetized by isoflurane inhalation, and right foot digit tips were amputated with microspring scissors, whereas the left foot digits were used as unamputated controls. The amputated digit tips were collected and stained with alizarine red to check the length of the bone section amputated.

Alizarin red staining of bones

Digits were collected, dehydrated in 100% ethanol for 24 hours, immersed in acetone for 24 hours, immersed in 1% potassium hydroxide for 4 hours, and stained for 48 hours in alizarin red staining solution (0.02% alizarin red, 1% potassium hydroxide). Tissue was cleared for 24 hours in 1% potassium hydroxide and conserved in glycerol.

Morphometric analyses of terminal phalanxes and nails

Digital images of freshly dissected nails and alizarin red–stained terminal phalanxes were taken with an Olympus DP70 digital camera, and the corresponding lengths (see Figure 3c and s) were measured using the ImageJ software (National Institutes of Health, Bethesda, MD). The number of individuals and values are described in Supplementary Table S1. For mean comparison, Student's *t* statistical tests were performed using the R software suite.

Whole-mount LacZ staining

Digits tips were harvested and cut transversely to facilitate solution penetration and whole-mount β-galactosidase staining using X-gal as a substrate. Whole-mount LacZ staining was performed overnight as described (Hogan et al., 1995). After staining, embryos were fixed in 4% paraformaldehyde and processed for further histological studies.

Tartrate-resistant acid phosphatase staining

For tartrate-resistant acid phosphatase staining, histological sections were deparaffinized, rehydrated, and incubated in 1% L-(+) tartaric acid (T-6521, Sigma-Aldrich), 1% naphthol AS-MX phosphate (N-4875, Sigma-Aldrich) and 1% and 0.06% Fast Red Violet LB Salt (F-3381, Sigma-Aldrich) at pH 5 for 4 hours at 37 °C. Preparations were counterstained with hematoxylin.

Analysis of apoptosis

Apoptosis was assessed with the TUNEL assay using the Fluorescent In Situ Cell Death Detection Kit (Roche, Mannheim, Germany) according to the manufacturer's instructions.

Single-cell RNA-sequencing data analysis

We used the single-cell RNA-sequencing datasets from uninjured and amputated digits 10, 14, and 28 days after amputation reported by Storer et al. (2020) (Gene Expression Omnibus GSE135985). Bioinformatic analyses were performed with Seurat (version 4) (Hao et al., 2021) following the author guidelines (https://satijalab.org/seurat/). Cells with unusually high and low numbers of unique feature counts or high mitochondrial counts were filtered out. Data were normalized and subsequently scaled. RunPCA was used for principal component analysis, and cells were clustered at a resolution of 0.6. Uniform manifold approximation and projection was used for nonlinear dimensional reduction. Cluster-specific markers were selected with a minimum average log fold change threshold of 0.25 among genes that were expressed in a minimum of 25% of the cells. Cluster identity was assigned using the following markers: *Pdgfra* + *Pdgfrb* + *Prrx2* for mesenchymal cells, *Pdgfrb* + *Rgs5* for vascular smooth muscle/pericytes, keratin genes *K5* + *K14* + *K17* for epithelial cells, *Tie1* + *Pecam1* for endothelial cells,

Cd14 + *Aif1* for immune cells/macrophages, and *Sox10* + *Plp1* for Schwann cells. Gene Ontology analyses were done with the enrichGO and the compareCluster functions of the clusterProfiler R package (Yu et al., 2012).

SUPPLEMENTARY REFERENCES

Akiyama H, Chaboissier MC, Martin JF, Schedl A, de Crombrugghe B. The transcription factor Sox9 has essential roles in successive steps of the chondrocyte differentiation pathway and is required for expression of Sox5 and Sox6. Genes Dev 2002;16:2813–28.

Dadhich RK, Barrionuevo FJ, Real FM, Lupiañez DG, Ortega E, Burgos M, et al. Identification of live germ-cell desquamation as a major mechanism of seasonal testis regression in mammals: a study in the Iberian mole (Talpa occidentalis)1. Biol Reprod 2013;88:101.

Hao Y, Hao S, Andersen-Nissen E, Mauck WM, Zheng S, Butler A, et al. Integrated analysis of multimodal single-cell data. Cell 2021;184:3573–87.e29.

Hayashi S, McMahon AP. Efficient recombination in diverse tissues by a tamoxifen-inducible form of Cre: a tool for temporally regulated gene activation/inactivation in the mouse. Dev Biol 2002;244:305–18.

Hogan B, Beddington R, Costantini F, Lacy E. Manipulating the mouse embryo. Cold Spring Harbor, NY: Cold Spring Harbor Laboratory Press; 1995.

Johnson GL, Masias EJ, Lehoczky JA. Cellular heterogeneity and lineage restriction during mouse digit tip regeneration at single-cell resolution. Dev Cell 2020;52:525–40.e5.

Soeda T, Deng JM. Crombrugghe B de, Behringer RR, Nakamura T, Akiyama H. Sox9-expressing precursors are the cellular origin of the cruciate ligament of the knee joint and the limb tendons. Genesis 2010;48:635–44.

Soriano P. Generalized lacZ expression with the ROSA26 Cre reporter strain. Nat Genet 1999;21:70–1.

Srinivas S, Watanabe T, Lin CS, William CM, Tanabe Y, Jessell TM, et al. Cre reporter strains produced by targeted insertion of EYFP and ECFP into the ROSA26 locus. BMC Dev Biol 2001;1:4.

Yu G, Wang LG, Han Y, He QY. clusterProfiler: an R package for comparing biological themes among gene clusters. OMICS 2012;16:284–7.

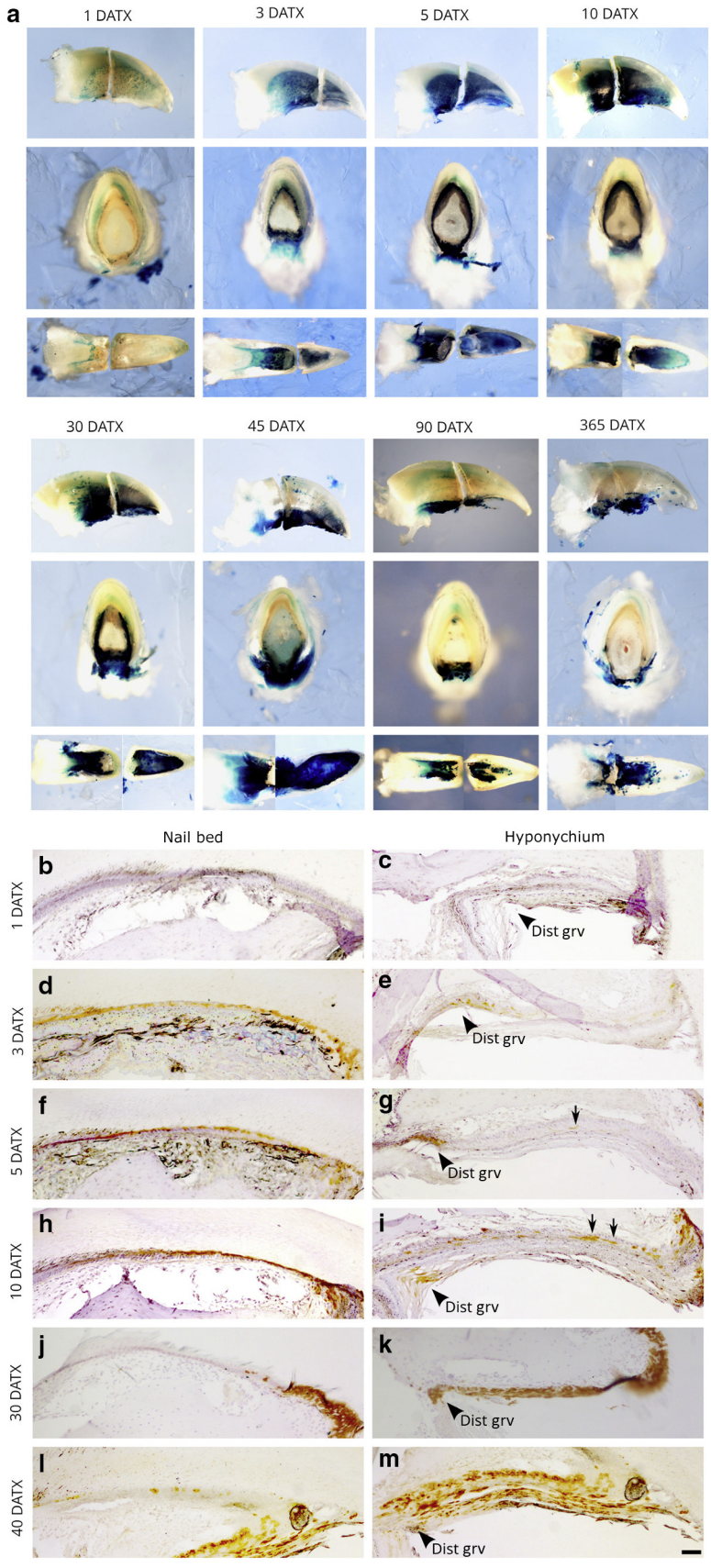

Supplementary Figure S1. Lineage tracing of *Sox9*-expressing cells in the mouse digit tip. (**a**) Whole-mount LacZ staining of *Sox9*$^{IRES\text{-}CreERT2}$;*R26R-LacZ* digit tip at various time points (DATX). The top panels show the lateral view, the central panels show the sagittal view, and the bottom panels show the ventral view of the nails. (**b–m**) EYFP immunohistochemistry of *Sox9*$^{IRES\text{-}CreERT2}$;*R26R-EYFP* digit tips at the indicated time points. Bar in **m** = 50 μm for **b–m**. DATX, day after tamoxifen administration; Dist Grv, distal groove.

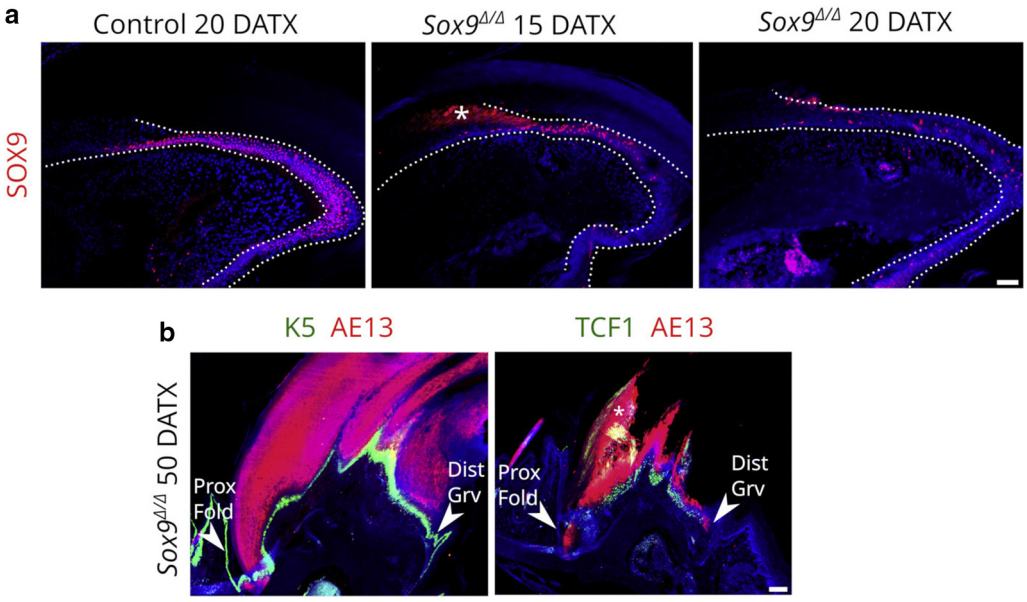

Supplementary Figure S2. Digit phenotype of *Sox9*$^{\Delta/\Delta}$ adult mice. (**a**) SOX9 immunofluorescence of control and *Sox9*$^{\Delta/\Delta}$ digit tips at the indicated time points. The dotted lines outline the nail epithelium domain and the hyponychium. (**b**) Double immunofluorescence for AE13 and either K5 or TCF1 in *Sox9*$^{\Delta/\Delta}$ digit-tip sections 50 DATXs. Asterisks indicate areas of nonspecific, autofluorescent background. Bars = 50 μm in **a** and 100 μm in **b**. DATX, day after tamoxifen administration; Dist Grv, distal groove; K5, keratin 5; Prox Fold, proximal fold; TCF1, T-cell factor 1.

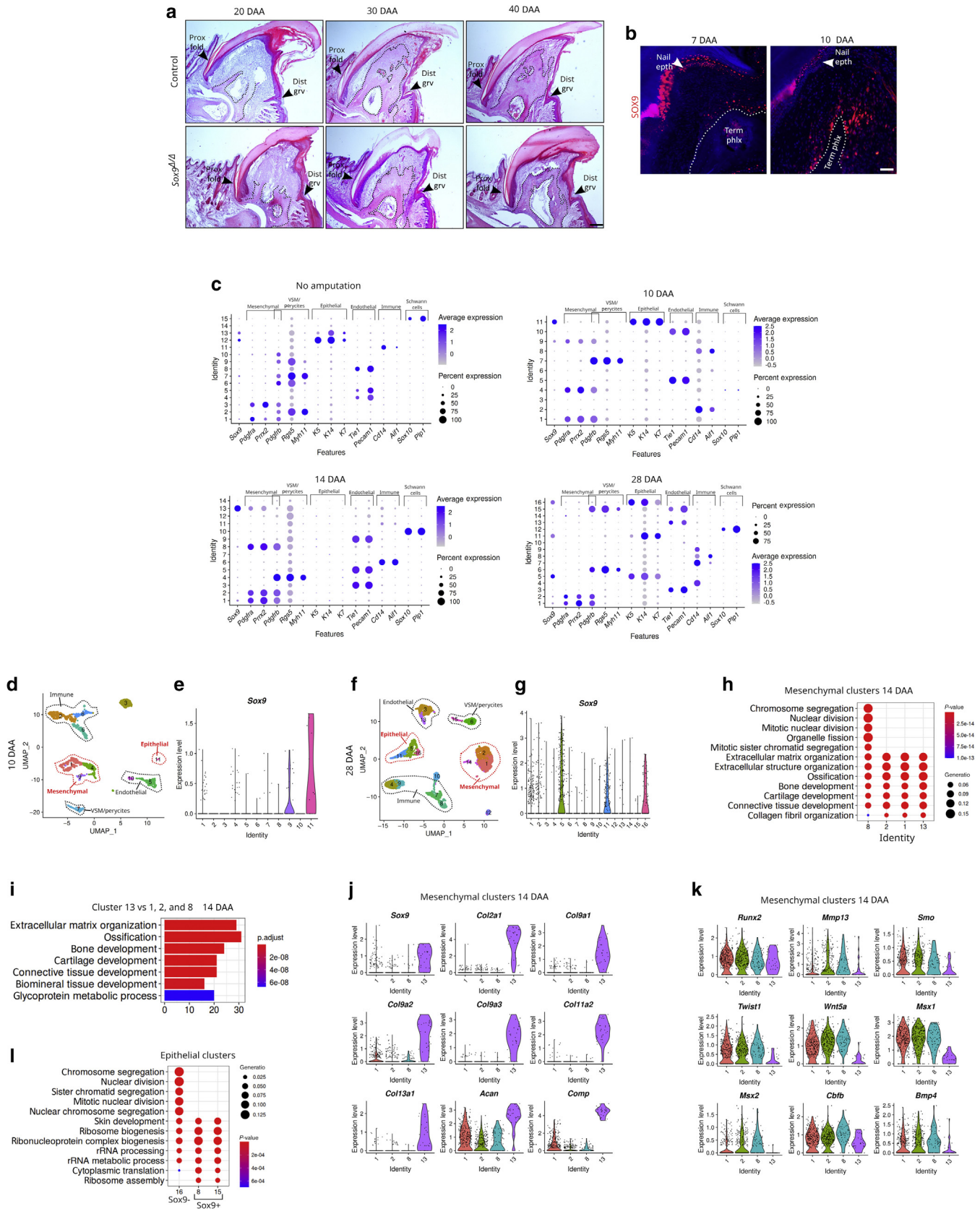

Supplementary Figure S3. Role of *Sox9* in mouse digit regeneration. (**a**) Histology of amputated control and *Sox9*$^{\Delta/\Delta}$ digit tips at various time points. Dotted lines outline the Term Phlx. (**b**) SOX9 immunofluorescence in control-amputated digit-tip sections at the indicated time points. The dotted lines outline the Term Phlx. (**c**) Dot plots showing the expression of cell-specific markers in the identified clusters of the scRNA-seq analysis at the indicated time points. (**d, f**) UMAP visualization of cell clusters identified in the scRNA-seq analysis of (**d**) 10 DAAs and (**f**) 28 DAAs amputated digit tips. The assignment of cell-type identities is depicted. (**e, g**) Violin plot showing *Sox9* expression in the identified clusters (**e**) 10 DAAs and (**g**) 28 DAAs. (**h**) Comparison of enriched biological processes

Supplementary Table S1. Quantification of Nail Length, Terminal Phalanx Length, and Percentage of RUNX2^{+} Cells

Experiment	Measure	Timepoint	Condition (1)	Mean (1)	SD (1)	n (1)	Condition (2)	Mean (2)	SD (2)	n (2)	Statistic	*P*-Value
Nonamputated	Nail length (mm)	50 DATX	Control	1.32	0.24	7	*Sox9*$^{\Delta/\Delta}$	2.92	0.33	7	Two-sample *t*-test	2.6×10^{-7}
Nonamputated	Terminal phalanx length (mm)	30 DATX	Control	1.22	0.05	4	*Sox9*$^{\Delta/\Delta}$	1.23	0.015	4	Two-sample *t*-test	0.74
Nonamputated	Terminal phalanx length (mm)	40 DATX	Control	1.19	0.04	4	*Sox9*$^{\Delta/\Delta}$	0.95	0.08	4	Two-sample *t*-test	0.002
Nonamputated	Terminal phalanx length (mm)	50 DATX	Control	1.23	0.04	6	*Sox9*$^{\Delta/\Delta}$	0.92	0.17	6	Two-sample *t*-test	0.0017
Amputated	Terminal phalanx length (mm)	50 DAAs	Control	1.36	0.14	6	*Sox9*$^{\Delta/\Delta}$	0.99	0.22	6	Two-sample *t*-test	0.0075
Amputated	% RUNX2+ cells	30 DAAs	Control	32.14	8.7	4	*Sox9*$^{\Delta/\Delta}$	16.4	8.06	4	Two-sample *t*-test	3.08×10^{-8}

Abbreviations: %, Percentage of; DAA, day after amputation; DATX, day after tamoxifen administration.

using the cell signature of identified mesenchymal clusters (clusters 1, 2, 8, and 13) 14 DAAs. (**i**) Gene Ontology analysis using the upregulated enriched genes in cluster 13 versus those in clusters 1, 2, and 8 14 DAAs. (**j**) Violin plot showing the expression of *Sox9* and chondrocyte extracellular matrix proteins in the mesenchymal clusters 14 DAAs. (**k**) Violin plot showing the expression of markers of osteoblast differentiation in the mesenchymal clusters 14 DAAs. (**l**) Comparison of enriched biological processes using the cell signature of identified epithelial clusters of the combined 11, 12, 14, and 17 DAAs and nonamputated scRNA-seq datasets generated by Johnson et al. (2020). Bars = 100 μm in **a** and 50 μm in **b**. DAA, day after amputation; Dist Grv, distal groove; Nail Epth, nail epithelium; Prox Fold, proximal fold; rRNA, ribosomal RNA; scRNA-seq, single-cell RNA sequencing; Term Phlx, terminal phalanx; UMAP, Uniform Manifold Approximation and Projection.